LANG, J. M., AUDIER, M., DUBOST, B. & SAINFORT, P. (1987). *J. Cryst. Growth*, **83**, 456–465.
LEBLANC, M., LE BAIL, A. & AUDIER, M. (1991). *Physica*. In the press.
LOISEAU, A. & LAPASSET, G. (1986). *J. Phys. (Paris)*, **47**, C3331–C3340.
LOISEAU, A. & LAPASSET, G. (1987). *Philos. Mag. Lett.* **56**, 165–171.
MACKAY, A. L. (1962). *Acta Cryst.* **15**, 916–918.
ROBINSON, W. T. & SHELDRICK, G. M. (1988). *Crystallographic Computing* 4: *Techniques and New Technologies*, edited by N. W. ISAACS & M. R. TAYLOR, pp. 366–377. Oxford Univ. Press.
SAMSON, S. (1968). *Structural Chemistry and Molecular Biology*, edited by A. RICH & N. DAVIDSON, pp. 687–717. San Francisco: Freeman.
SHECHTMAN, D., BLECH, I., GRATIAS, D. & CAHN, J. W. (1984). *Phys. Rev. Lett.* **53**, 1951–1954.
SHELDRICK, G. M. (1976). *SHELX*76. Program for crystal structure determination. Univ. of Cambridge, England.
SHELDRICK, G. M. (1985). *Crystallographic Computing* 3, edited by G. M. SHELDRICK, C. KRÜGER & R. GODDARD, pp. 175–189. Oxford Univ. Press.
SHELDRICK, G. M. (1990). *Acta Cryst.* A**46**, 467–473.
SHOEMAKER, C. B., KESZLER, D. A. & SHOEMAKER, D. P. (1989). *Acta Cryst.* B**45**, 13–20.

Acta Cryst. (1991). B**47**, 457–462

Structures of Orthorhombic and Monoclinic $Ni_3(AsO_4)_2$

BY J. BARBIER AND C. FRAMPTON

Department of Chemistry, McMaster University, 1280 Main Street West, Hamilton, Ontario L8S 4M1, Canada

(*Received* 24 *September* 1990; *accepted* 6 *March* 1991)

Abstract

The crystal structures of two hydrothermally grown polymorphs of nickel orthoarsenate *o*- and *m*-$Ni_3(AsO_4)_2$ have been determined by single-crystal X-ray diffraction. Crystal data: *o*-$Ni_3(AsO_4)_2$, M_r = 454·01, orthorhombic, *Cmca*, $Z = 4$, $F(000) = 859{\cdot}95$, λ(Mo $K\alpha$) = 0·71069 Å, $T = 295$ (1) K, a = 5·943 (2), b = 11·263 (4), c = 8·164 (3) Å, V = 546·5 (3) Å^3, $D_x = 5{\cdot}517$ g cm^{-3}, μ(Mo $K\alpha$) = 228·69 cm^{-1}, $R = 0{\cdot}035$, $wR = 0{\cdot}030$ for 439 independent reflections; *m*-$Ni_3(AsO_4)_2$, monoclinic, $P2_1/c$, $Z = 4$, $F(000) = 859{\cdot}95$, λ(Mo $K\alpha$) = 0·71069 Å, T = 295 (1) K, $a = 5{\cdot}764$ (1), $b = 9{\cdot}559$ (2), c = 10·194 (2) Å, $\beta = 92{\cdot}95°$, $V = 560{\cdot}9$ (1) Å^3, D_x = 5·374 g cm^{-3}, μ(Mo $K\alpha$) = 222·76 cm^{-1}, R = 0·040, $wR = 0{\cdot}031$ for 1640 independent reflections. The crystal chemistry of nickel orthoarsenate is intermediate between those of the corresponding phosphate and vanadate, and its dimorphism is closely related to the olivine–spinel phase relations.

1. Introduction

Following the earlier work of Calvo and co-workers on the crystal chemistry of cobalt arsenates (Krishnamachari & Calvo, 1970*a*,*b*, 1974; Ozog, Krishnamachari & Calvo, 1970), a similar study of the NiO–As_2O_5 system has recently been undertaken. Interest in this system also stems from the recognition of structural relationships between some of the nickel arsenate phases and a newly identified series of germanate compounds (Barbier, 1987; Fleet & Barbier, 1988, 1989).

Initial crystal-growth experiments using a nickel arsenate hydrate melt led to the synthesis and structure determination of the Ni-rich phase $Ni_{8.5}As_3O_{16}$ (Fleet & Barbier, 1989), the synthetic analog of the mineral aerugite (Davis, Hey & Kingsbury, 1965) and isostructural with the corresponding magnesium and cobalt arsenates (Bless & Kostiner, 1973; Krishnamachari & Calvo, 1970*a*). Attempts to grow single crystals of the $Ni_3(AsO_4)_2$ phase [*i.e.* xanthiosite, the other mineral identified by Davis *et al.* (1965)] were unsuccessful using the same technique. Further experiments were therefore based on hydrothermal crystal growth using a powder of composition $Ni_3(AsO_4)_2.8H_2O$ as starting material. These experiments yielded several anhydrous and hydrated nickel arsenates including the two $Ni_3(AsO_4)_2$ polymorphs which are the subject of the present paper: monoclinic *m*-$Ni_3(AsO_4)_2$, or synthetic xanthiosite, isostructural with $Co_3(AsO_4)_2$ (Krishnamachari & Calvo, 1970*b*), and orthorhombic *o*-$Ni_3(AsO_4)_2$ with no cobalt analog known at present but isostructural with the vanadates $Ni_3(VO_4)_2$ and $Co_3(VO_4)_2$ (Sauerbrei, Faggiani & Calvo, 1973).

2. Hydrothermal crystal growth

The starting material for the hydrothermal growth experiments consisted of a commercial powder of nominal composition $Ni_3(AsO_4)_2.8H_2O$ (synthetic

0108-7681/91/040457-06$03.00

annabergite from K & K Rare Chemicals, water content checked by TGA). Approximately 100 mg were sealed in a gold capsule, without any extra water, and the capsule was then loaded into an externally heated cold-seal hydrothermal reactor. A number of experimental runs were carried out at temperatures between 873 and 1093 K, the pressure being kept constant at $1\cdot0 \pm 0\cdot1$ kbar over the duration of the run (typically 3–4 days).

The run products always contained a mixture of crystalline phases which could easily be distinguished by the colour and morphology of the crystals. For instance, o-$Ni_3(AsO_4)_2$ crystallized as thin long yellow–green prisms whereas m-$Ni_3(AsO_4)_2$ formed short stubby green prisms (*cf.* Fig. 1). Furthermore, these two polymorphs were obtained over different temperature ranges: the orthorhombic form was only found in the low-temperature runs (873–923–988 K) whereas the monoclinic crystals only formed (in small numbers) at higher temperature (1023–1043 K). The other phases recovered in these experiments included $Ni_3(AsO_4)_2.H_2O$ [previously reported by Palazzi & Guérin (1978)] in the 873 K run, three new (possibly) hydrated nickel arsenates at intermediate temperatures and $Ni_{8\cdot5}As_3O_{16}$ (aerugite) plus NiO in the 1073–1093 K runs.

3. Data collection and structure solutions

Data for the determination of m-$Ni_3(AsO_4)_2$ are given in parentheses. A yellow–green (green) prism, $0\cdot48 \times 0\cdot06 \times 0\cdot03$ mm ($0\cdot16 \times 0\cdot13 \times 0\cdot08$ mm), of o-$Ni_3(AsO_4)_2$ [m-$Ni_3(AsO_4)_2$] was selected and mounted on the tip of a glass fibre with use of epoxy cement. Unit-cell parameters at 295 K were obtained from a least-squares fit of χ, φ and 2θ for 15 (15) reflections in the range $20\cdot1 < 2\theta < 28\cdot5°$ ($24\cdot4 < 2\theta < 28\cdot8°$) recorded on a Nicolet $P3$ (Syntex $P2_1$) diffractometer using graphite-monochromated Mo $K\alpha$ radiation. Intensity data were also recorded on the same instrument at 295 K with a coupled θ(crystal)–2θ(counter) scan, scan range $K\alpha_1 - 1\cdot0$ to $K\alpha_2 + 1\cdot0°$, for 918 (1891) reflections in the hemisphere h, k, $\pm l$, $0 \le h \le 8$, $0 \le k \le 15$, $-11 \le l \le 11$ ($0 \le h \le 8$, $0 \le k \le 13$, $-14 \le l \le 14$), with $2\theta \le 60°$. The range of scan rates used was 2·02 (3·91) to 9·77 (29·3)° min^{-1} in 2θ. The ratio background time to scan time was 1:1. Two standard reflections, 244, 1·25% and $11\bar{2}$, 0·91% ($25\bar{2}$, 1·33% and 333, 1·21%), monitored every 48 reflections showed no sign of crystal decomposition or instrument instability. The data were corrected for Lorentz–polarization effects and empirically for absorption effects by ψ scans of 15 reflections with use of the program *TAPER* (Calabrese & Burnett, 1980). Absorption coefficient limits $1\cdot76$ ($3\cdot93$) $\le A^* \le 3\cdot91$ ($11\cdot361$). Reflections with $3\sigma(I) \ge I \ge -3\sigma(I)$ were treated by the method of French & Wilson (1978). Systematically absent reflections, 71 (106), were excluded and 408 (145) symmetry-equivalent data were then averaged, $R_{int} = 0\cdot0289$ ($0\cdot0344$), to give 439 (1640) unique reflections, 404 (1347) with $I > 2\cdot5\sigma(I)$.

Both structures were solved using conventional Patterson and Fourier techniques and refined by least-squares calculations minimizing $\sum w(|F_o| - |F_c|)^2$ $\{w = [\sigma^2(F)]^{-1}\}$ with use of the *XTAL* suite of programs (Hall & Stewart, 1989) on a VAX 6420 computer. For o-$Ni_3(AsO_4)_2$ and m-$Ni_3(AsO_4)_2$, the refinement was terminated when the maximum shift/e.s.d. in the final cycle was 0·0001. An isotropic secondary-extinction correction, $g = 0\cdot40$ (2) [$0\cdot060$ (2)], was included in the refinement. Final $R = 0\cdot035$ ($0\cdot040$), $wR = 0\cdot030$ ($0\cdot031$) and $S = 3\cdot703$

(*a*)

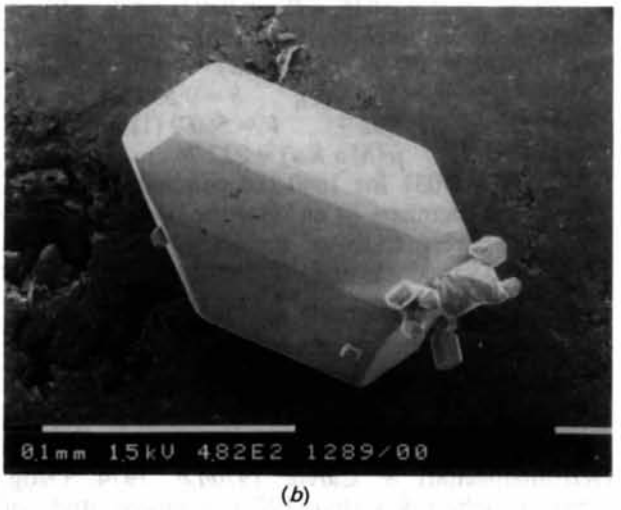

(*b*)

Fig. 1. SEM photographs of hydrothermally grown $Ni_3(AsO_4)_2$ crystals: (*a*) thin long yellow-green prisms of o-$Ni_3(AsO_4)_2$ and (*b*) stubby green prisms of m-$Ni_3(AsO_4)_2$. The elongation direction is parallel to the crystallographic a axis in both cases. Similar crystals were used for the structure refinements.

Table 1. *Positional and equivalent isotropic thermal parameters* ($Å^2$) *for* o-$Ni_3(AsO_4)_2$ *and* m-$Ni_3(AsO_4)_2$ *with e.s.d.'s in parentheses*

	Equipoint	x	y	z	U_{eq}
o-$Ni_3(AsO_4)_2$ (*Cmca*)					
Ni(1)	4(*a*)	0·0	0·0	0·0	0·0065 (7)*
Ni(2)	8(*e*)	0·25	0·1335 (1)	0·25	0·0063 (7)*
As	8(*f*)	0·0	0·37586 (7)	0·11627 (9)	0·0047 (4)*
O(1)	8(*f*)	0·0	0·2528 (5)	0·2333 (6)	0·008 (2)*
O(2)	8(*f*)	0·0	−0·0026 (5)	0·2502 (8)	0·007 (2)*
O(3)	16(*g*)	0·2647 (8)	0·1206 (4)	−0·0007 (5)	0·007 (2)*
m-$Ni_3(AsO_4)_2$ ($P2_1/c$)					
Ni(1)	4(*e*)	−0·11623 (13)	0·13508 (8)	−0·46619 (7)	0·0055 (3)†
Ni(2)	4(*e*)	−0·35785 (13)	0·13685 (8)	−0·21622 (7)	0·0054 (3)†
Ni(3)	4(*e*)	0·35985 (13)	0·12278 (8)	0·05781 (7)	0·0053 (3)†
As(1)	4(*e*)	0·36612 (10)	0·15639 (6)	0·38124 (5)	0·0043 (3)†
As(2)	4(*e*)	−0·12618 (10)	0·05552 (6)	0·20430 (5)	0·0040 (2)†
O(1)	4(*e*)	0·3834 (7)	0·2253 (4)	0·2291 (3)	0·006 (2)†
O(2)	4(*e*)	0·6028 (7)	0·2437 (4)	0·4526 (4)	0·007 (2)†
O(3)	4(*e*)	0·1556 (6)	0·2334 (4)	0·4649 (4)	0·005 (2)†
O(4)	4(*e*)	−0·3666 (7)	0·0183 (4)	0·6187 (4)	0·008 (2)†
O(5)	4(*e*)	0·3745 (6)	0·4898 (4)	0·3771 (4)	0·005 (2)†
O(6)	4(*e*)	−0·1328 (7)	0·2317 (4)	0·1933 (4)	0·007 (2)†
O(7)	4(*e*)	0·1127 (7)	−0·0050 (5)	0·1330 (4)	0·006 (2)†
O(8)	4(*e*)	0·1191 (7)	0·5075 (5)	0·1362 (4)	0·007 (2)†

* $U_{eq} = \frac{1}{3}(U_{11} + U_{22} + U_{33})$.
† $U_{eq} = \frac{1}{3}(U_{11} + U_{22} + U_{33} + 2\cos\beta U_{13})$.

(1·817) for 38 (119) variables. A final difference map showed electron density maximum 1·8 (1·7), minimum −1·8 (−1·3) e $Å^{-3}$. Throughout the refinements, scattering curves were taken from those stored within the program and anomalous-dispersion corrections were applied to the curves for nickel and arsenic. Final atomic positional parameters are given in Table 1.* Bond lengths and bond angles are given in Tables 2 and 3. Further cycles of refinement with variable Ni and As populations did not indicate any significant deviation from the $Ni_3As_2O_8$ composition.

4. Description of the o-$Ni_3(AsO_4)_2$ structure

This structure (Fig. 2) is based on an approximate cubic close packing (eutaxy) of O atoms with $\frac{3}{8}$ of the octahedral sites and $\frac{1}{4}$ of the tetrahedral sites filled with Ni and As atoms respectively. The NiO_6 octahedra are joined by edge-sharing with one another but only share corners with the AsO_4 tetrahedra. The deviation from ideal close packing can be estimated from the axial ratios $c/a = 1·374$ and $b/a = 1·895$ compared to their ideal values of $\sqrt{2}$ and 2.

The full coordination of the o-$Ni_3(AsO_4)_2$ structure can be written as $^{VI}Ni(1)^{VI}Ni(2)_2{}^{IV}As_2{}^{III}O(1)_2$-$^{IV}O(2)_2{}^{III}O(3)_4$ where O(1) and O(3) are in threefold coordination (2Ni + As) whereas O(2) is in fourfold

* Lists of structure factors and anisotropic thermal parameters have been deposited with the British Library Document Supply Centre as Supplementary Publication No. SUP 54039 (16 pp.). Copies may be obtained through The Technical Editor, International Union of Crystallography, 5 Abbey Square, Chester CH1 2HU, England.

Table 2. *Bond lengths* (Å), *strengths* (*s*) *and angles* (°) *in* o-$Ni_3(AsO_4)_2$

Ni(1)—O(2)	2·043 (7) (×2)	As—O(1)	1·684 (6)
Ni(1)—O(3)	2·079 (5) (×4)	As—O(2)*e*	1·751 (6)
		As—O(3)*f*	1·687 (4) (×2)
Ni(2)—O(1)	2·007 (4) (×2)		
Ni(2)—O(2)	2·135 (4) (×2)		
Ni(2)—O(3)	2·054 (4) (×2)		

	O(1)	O(2)	O(3)	Σs
Ni(1)		0·350 (×2)	0·318 (×4)	1·97
Ni(2)	0·385 (×2)	0·273 (×2)	0·339 (×2)	1·99
As	1·251	1·047	1·241 (×2)	4·78
Σs	2·02	1·94	1·90	

O(2)—Ni(1)—O(2)*a*	180·0	O(1)—Ni(2)—O(1)*d*	96·04 (18)
O(2)—Ni(1)—O(3)	90·69 (15) (×4)	O(1)—Ni(2)—O(2)	88·01 (16) (×2)
O(2)—Ni(1)—O(3)*a*	89·31 (15) (×4)	O(1)—Ni(2)—O(2)*d*	174·53 (21) (×2)
O(3)—Ni(1)—O(3)*a*	180·0	O(1)—Ni(2)—O(3)	90·63 (20) (×2)
O(3)—Ni(1)—O(3)*b*	98·37 (18) (×2)	O(1)—Ni(2)—O(3)*d*	94·81 (20) (×2)
O(3)—Ni(1)—O(3)*c*	81·63 (18) (×2)	O(2)—Ni(2)—O(2)*d*	88·21 (16)
O(3)*b*—Ni(1)—O(3)*c*	180·0	O(2)—Ni(2)—O(3)	88·81 (22) (×2)
O(1)—As—O(2)*e*	106·9 (3)	O(2)—Ni(2)—O(3)*d*	85·35 (22) (×2)
O(1)—As—O(3)*f*	109·66 (18) (×2)	O(3)—Ni(2)—O(3)*d*	171·87 (19)
O(2)*e*—As—O(3)*f*	109·26 (18) (×2)		
O(3)*f*—As—O(3)*g*	111·95 (21)		

Symmetry code: (*a*) $-x, -y, -z$; (*b*) $-x, y, z$; (*c*) $x, -y, -z$; (*d*) $\frac{1}{2}-x, y, \frac{1}{2}-z$; (*e*) $-x, \frac{1}{2}+y, \frac{1}{2}-z$; (*f*) $\frac{1}{2}-x, \frac{1}{2}-y, -z$; (*g*) $-\frac{1}{2}+x, \frac{1}{2}-y, -z$.

Table 3. *Bond lengths* (Å) *and angles* (°) *in* m-$Ni_3(AsO_4)_2$

Ni(1)—O(2)*a*	2·061 (4)	Ni(2)—O(1)*e*	2·046 (4)	Ni(3)—O(1)	2·001 (4)
Ni(1)—O(3)*b*	1·986 (4)	Ni(2)—O(2)*e*	2·088 (4)	Ni(3)—O(2)*c*	2·212 (4)
Ni(1)—O(4)*b*	2·051 (4)	Ni(2)—O(4)*b*	2·027 (4)	Ni(3)—O(3)*c*	2·014 (4)
Ni(1)—O(6)*c*	2·071 (4)	Ni(2)—O(5)*e*	2·214 (4)	Ni(3)—O(5)*g*	2·072 (4)
Ni(1)—O(8)*d*	2·119 (4)	Ni(2)—O(6)*c*	2·058 (4)	Ni(3)—O(5)*c*	2·139 (4)
Ni(1)—O(8)*c*	2·154 (4)	Ni(2)—O(7)*f*	2·045 (4)	Ni(3)—O(7)	2·055 (4)
As(1)—O(1)	1·693 (4)	As(2)—O(5)*i*	1·735 (4)		
As(1)—O(2)	1·728 (4)	As(2)—O(6)	1·689 (4)		
As(1)—O(3)	1·688 (4)	As(2)—O(7)	1·692 (4)		
As(1)—O(4)*h*	1·670 (4)	As(2)—O(8)*i*	1·688 (4)		

O(2)*a*—Ni(1)—O(3)*b*	103·73 (16)	O(1)—Ni(3)—O(2)*c*	97·14 (16)
O(2)*a*—Ni(1)—O(4)*b*	83·57 (16)	O(1)—Ni(3)—O(3)*c*	95·05 (16)
O(2)*a*—Ni(1)—O(6)*c*	86·48 (16)	O(1)—Ni(3)—O(5)*g*	90·30 (16)
O(2)*a*—Ni(1)—O(8)*d*	89·35 (16)	O(1)—Ni(3)—O(5)*c*	173·79 (16)
O(2)*a*—Ni(1)—O(8)*c*	167·26 (16)	O(1)—Ni(3)—O(7)	89·00 (16)
O(3)*b*—Ni(1)—O(4)*b*	172·68 (16)	O(2)*c*—Ni(3)—O(3)*c*	75·39 (15)
O(3)*b*—Ni(1)—O(6)*c*	93·19 (16)	O(2)*c*—Ni(3)—O(5)*g*	91·90 (16)
O(3)*b*—Ni(1)—O(8)*d*	87·50 (16)	O(2)*c*—Ni(3)—O(5)*c*	79·56 (15)
O(3)*b*—Ni(1)—O(8)*c*	88·99 (16)	O(2)*c*—Ni(3)—O(7)	172·82 (15)
O(4)*b*—Ni(1)—O(6)*c*	86·64 (17)	O(3)*c*—Ni(3)—O(5)*g*	166·72 (16)
O(4)*b*—Ni(1)—O(8)*d*	93·20 (16)	O(3)*c*—Ni(3)—O(5)*c*	89·24 (16)
O(4)*b*—Ni(1)—O(8)*c*	83·72 (16)	O(3)*c*—Ni(3)—O(7)	100·45 (16)
O(6)*c*—Ni(1)—O(8)*d*	175·82 (16)	O(5)*g*—Ni(3)—O(5)*c*	84·58 (15)
O(6)*c*—Ni(1)—O(8)*c*	93·53 (16)	O(5)*g*—Ni(3)—O(7)	91·78 (16)
O(8)*d*—Ni(1)—O(8)*c*	90·60 (16)	O(15)*c*—Ni(3)—O(7)	94·65 (16)
O(1)*e*—Ni(2)—O(2)*e*	76·33 (15)	O(1)—As(1)—O(2)	96·63 (19)
O(1)*e*—Ni(2)—O(4)*b*	98·46 (16)	O(1)—As(1)—O(3)	111·79 (19)
O(1)*e*—Ni(2)—O(5)*e*	87·44 (15)	O(1)—As(1)—O(4)*h*	112·91 (20)
O(1)*e*—Ni(2)—O(6)*c*	87·26 (16)	O(2)—As(1)—O(3)	98·57 (19)
O(1)*e*—Ni(2)—O(7)*f*	171·30 (16)	O(2)—As(1)—O(4)*h*	118·79 (20)
O(2)*e*—Ni(2)—O(4)*b*	172·32 (17)	O(3)—As(1)—O(4)*h*	115·93 (20)
O(2)*e*—Ni(2)—O(5)*e*	80·62 (16)		
O(2)*e*—Ni(2)—O(6)*c*	97·67 (16)	O(5)*i*—As(2)—O(6)	108·31 (19)
O(2)*e*—Ni(2)—O(7)*f*	95·59 (16)	O(5)*i*—As(2)—O(7)	109·90 (19)
O(4)*b*—Ni(2)—O(5)*e*	93·63 (16)	O(5)*i*—As(2)—O(8)*i*	109·93 (19)
O(4)*b*—Ni(2)—O(6)*c*	87·61 (16)	O(6)—As(2)—O(7)	109·19 (20)
O(4)*b*—Ni(2)—O(7)*f*	89·26 (17)	O(6)—As(2)—O(8)*i*	109·56 (20)
O(5)*e*—Ni(2)—O(6)*c*	174·67 (16)	O(7)—As(2)—O(8)*i*	109·92 (20)
O(5)*e*—Ni(2)—O(7)*f*	88·08 (16)		
O(6)*c*—Ni(2)—O(7)*f*	97·12 (16)		

Symmetry code: (*a*) $-1+x, y, -1+z$; (*b*) $x, y, -1+z$; (*c*) $x, \frac{1}{2}-y, -\frac{1}{2}+z$; (*d*) $-x, -\frac{1}{2}+y, -\frac{1}{2}-z$; (*e*) $-1+x, \frac{1}{2}-y, -\frac{1}{2}+z$; (*f*) $-x, -y, -z$; (*g*) $1-x, -\frac{1}{2}+y, \frac{1}{2}-z$; (*h*) $-x, -y, 1-z$; (*i*) $-x, -\frac{1}{2}+y, \frac{1}{2}-z$.

coordination (3Ni + As) (*cf.* Fig. 2). As expected from bond-valence/bond-length correlations, the longest bonds in the structure are those involving O(2) (*cf.* Table 2). All bond-valence sums [calculated from the parameters derived by Altermatt & Brown (1985)] are close to their expected values (*cf.* Table 2) but individual bond lengths and angles show significant distortion of all coordination polyhedra, only slightly larger than those observed in the isostructural vanadate $Ni_3(VO_4)_2$ (Sauerbrei *et al.*, 1973).

As pointed out previously by Krishnamachari & Calvo (1971) in the case of the isostructural Mg orthovanadate, the *o*-$Ni_3(AsO_4)_2$ structure is simply related to the spinel structure type. This relationship is best seen using the projection of Fig. 2 which is equivalent to the ⟨110⟩ projection of the spinel structure [see, for instance, Fig. 1 in Hyde, White, O'Keeffe & Johnson (1982)]. The *o*-$Ni_3(AsO_4)_2$ unit cell contains cation-deficient spinel slabs stacked along the *b* direction, the Ni vacancies being ordered along empty octahedral rows parallel to the *a* axis. Adjacent slabs are separated by (020) antiphase boundaries with a displacement vector equal to *a*/2 that leaves the cubic close-packed oxygen array essentially invariant. In an A_2BO_4 spinel structure, equivalent slabs are stoichiometric and are related by a simple translation along the ⟨$\bar{1}$10⟩ direction. In respect to this structural relationship, it is relevant to point out the existence of a low-temperature pseudo-cubic spinel-like form of $Co_3(VO_4)_2$ (Joubert & Durif, 1964) that has no antiphase boundaries and a different distribution of the octahedral vacancies.

5. Description of the *m*-$Ni_3(AsO_4)_2$ (xanthiosite) structure

The xanthiosite structure (Fig. 3) is based on a mixed hexagonal–cubic oxygen packing with an *hc* stacking sequence in the *b* direction leading to a four-layer repeat. Again, Ni and As atoms occupy $\frac{3}{8}$ and $\frac{1}{4}$ of the octahedral and tetrahedral sites respectively but some edge sharing occurs in the hexagonal layers between the NiO_6 and AsO_4 polyhedra. Whereas the oxygen packing is clearly distorted from ideal close packing (eutaxy), the average height of a layer, as measured by the ratio $b/(2a \sin\beta) = 0{\cdot}830$, remains close to its ideal value of $\sqrt{\frac{2}{3}} = 0{\cdot}816$.

All atoms are in general positions (*cf.* Table 1) and the full coordination of the *m*-$Ni_3(AsO_4)_2$ structure is given by $^{VI}Ni(1)^{VI}Ni(2)^{VI}Ni(3)^{VI}As(1)^{IV}As(2)^{III}O(1)$-$^{IV}O(2)^{III}O(3)^{III}O(4)^{IV}O(5)^{III}O(6)^{III}O(7)^{III}O(8)$ (*cf.* Fig. 3). As in *o*-$Ni_3(AsO_4)_2$, the four-coordinated (3Ni + As) O(2) and O(5) oxygen atoms involve the longest bonds in the structure (*cf.* Table 3). Both the bond lengths and bond angles indicate significant distortion of all coordination polyhedra (much greater than in the orthorhombic form) except for the $As(2)O_4$ tetrahedron. Nevertheless, all bond-valence

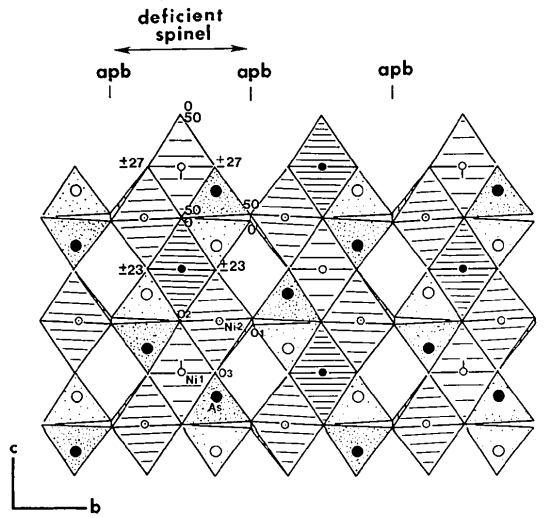

Fig. 2. The crystal structure of orthorhombic *o*-$Ni_3(AsO_4)_2$ viewed along the *a* direction. Large and small circles represent As and Ni atoms respectively. Open, filled and dotted circles are at heights 0, 50 and ±25 (in units of *a*/100). The O atoms at the corners of the polyhedra have been omitted and only their heights are indicated. The structure is based on a cubic close-packed oxygen array and consists of deficient-spinel slabs related by antiphase boundaries. Note the empty octahedral rows parallel to the *a* direction.

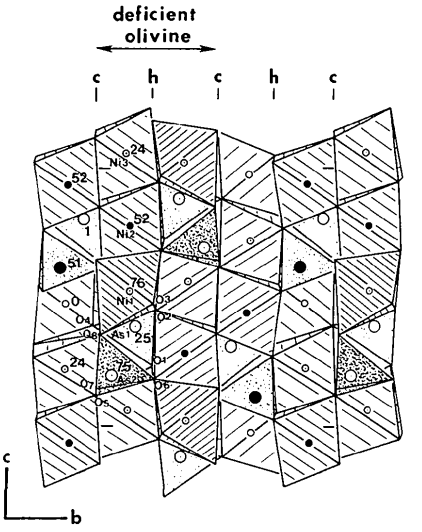

Fig. 3. The crystal structure of monoclinic *m*-$Ni_3(AsO_4)_2$ projected onto the (100) plane. Large and small circles represent As and Ni atoms, the O atoms at the corners of the polyhedra have been omitted. Open, filled and dotted circles are at heights of approximately 0, 50 and 25 *or* 75 (in units of d_{100}/100). Note that the atom heights have all been shifted by −12 for easier comparison with Fig. 1. For reason of clarity, the heights of the O atoms have also been omitted. The structure is based on a mixed *hc* approximate close-packing of O atoms and consists of deficient-olivine slabs centered on the *h* layers. Note that all (010) layers are identical and have $Ni_3As_2O_8$ stoichiometry.

sums remain close (within 5%) to their expected values and similar bonding geometries have also been observed in isostructural $Co_3(AsO_4)_2$ (Krishnamachari & Calvo, 1970*b*).

As shown in Fig. 3, the xanthiosite structure contains slabs of cation-deficient olivine structure: these slabs consist of double hexagonally packed (*h*) layers stacked in such a way that adjacent slabs are in cubic (*c*) packing. Ni vacancies are ordered in all individual (010) layers which then have $Ni_3As_2O_8$ stoichiometry (note the Ni atoms at heights of approximately $\frac{1}{4}$, $\frac{1}{2}$, $\frac{3}{4}$ *or* 0, $\frac{1}{4}$, $\frac{1}{2}$). [By contrast, in the A_2BO_4 olivine structure type, all available octahedral sites are filled (with *A* atoms at heights of $\frac{1}{4}$, $\frac{3}{4}$, 0 *and* $\frac{1}{2}$ in all layers) and the layer stacking corresponds to a simple hexagonal close packing (*h*).] These olivine-like slabs present in the xanthiosite structure correspond, in fact, to the sarcopside $(Fe,Zn)_3(PO_4)_2$ structure type, also adopted by $Ni_3(PO_4)_2$ (Calvo & Faggiani, 1975). Both xanthiosite and sarcopside are, therefore, built of the same $A_3B_2O_8$ layers but, whereas the layer stacking is (*hc*) in the former, it is simply (*h*) in the latter as in olivine itself. These two structure types can then be regarded as members of a structural family with other members possibly existing in systems such as *m*-$Ni_3(AsO_4)_2$–$Ni_3(PO_4)_2$.

6. Discussion

Among the various structure types reported for the orthoarsenates $M_3(AsO_4)_2$ (M = Mg, Mn, Co, Ni, Cu, Cd) (Krishnamachari & Calvo, 1973, 1970*b*; Krishnamachari, 1970; Gopal, Rutherford & Robertson, 1980; Davis *et al.*, 1965; Poulsen & Calvo, 1968; Hawthorne, 1986; Engle & Klee, 1970), the dimorphism of $Ni_3(AsO_4)_2$ described here is so far unique. On the one hand, the *o*-$Ni_3(AsO_4)_2$ phase is the first example of an arsenate adopting this spinel-related structure which is common among the orthovanadates $M_3(VO_4)_2$ (M = Mg, Ni, Co, Cu, Zn) (Krishnamachari & Calvo, 1971; Sauerbrei *et al.*, 1973; Shannon & Calvo, 1972). On the other hand, the *m*-$Ni_3(AsO_4)_2$ (xanthiosite) structure is closely related to that of sarcopside, an olivine derivative, adopted by several orthophosphates including $Ni_3(PO_4)_2$ (Moore, 1972; Berthet, Joubert & Bertaut, 1972; Calvo & Faggiani, 1975). Clearly, its dimorphism makes nickel orthoarsenate a structural intermediate between the corresponding vanadate and phosphate.

The dimorphism of $Ni_3(AsO_4)_2$ is also relevant to the well-known phase relations between the olivine and spinel structure types. For example, the spinel and olivine forms of Mg_2GeO_4 are low-/high-temperature (as well as high-/low-pressure) forms respectively (Dachille & Roy, 1960; Hensen, 1977). Similarly, the stability of the spinel-related orthorhombic form of $Ni_3(AsO_4)_2$ seems to be limited to low temperature: firstly, it crystallized in the low-temperature hydrothermal runs only (*cf.* §2) and secondly, during dehydration reactions of synthetic annabergite $Ni_3(AsO_4)_2.8H_2O$, both the *o*- and *m*-$Ni_3(AsO_4)_2$ phases were obtained at 948 K, but only the latter remained when the temperature was raised to 998 K. The difference in the calculated densities of *o*- and *m*-$Ni_3(AsO_4)_2$ (5·52 and 5·37 g cm^{-3}) is also consistent with the densities of spinel and olivine polymorphs of silicates and germanates (*e.g.* 4·38 and 4·03 g cm^{-3} for Mg_2GeO_4) suggesting that, like spinel, the *o*-$Ni_3(AsO_4)_2$ structure may also be the stable high-pressure form.

As described above, the structure of xanthiosite [*m*-$Ni_3(AsO_4)_2$] is built up of cation-deficient olivine layers of $Ni_3As_2O_8$ composition, identical to those in sarcopside. Similar layers are also found in the structure of aerugite ($Ni_{8.5}As_3O_{16}$) albeit with a different composition, $Ni_{3.67}As_2O_8$, and regularly intergrown with deficient rock-salt layers, $Ni_{4.87}AsO_8$ (Fleet & Barbier, 1989). This structural relation between xanthiosite and aerugite may be relevant to the fact that the former readily transforms into the latter, *via* loss of As_2O_5, when heated in air of a few minutes at 1373 K. The examination of partially transformed xanthiosite by transmission electron microscopy showed a few (010) planar faults possibly associated with the formation of an intermediate phase. No such phase has yet been observed in the NiO–As_2O_5 system (Taylor & Heyding, 1958; Davis *et al.*, 1965) but in the CoO–As_2O_5 system, the $Co_7As_{3.6}O_{16}$ olivine-like phase described by Krishnamachari & Calvo (1974) has a Co/As ratio intermediate between those of xanthiosite ($M_3As_2O_8$) and aerugite ($M_{8.5}As_3O_{16}$). The possible existence of a similar phase in the nickel system is now being investigated.

This work was supported by an operating grant to JB from the National Science and Engineering Research Council of Canada.

References

ALTERMATT, D. & BROWN, I. D. (1985). *Acta Cryst.* B**41**, 240–244.
BARBIER, J. (1987). *Acta Cryst.* B**43**, 422–429.
BERTHET, G., JOUBERT, J. C. & BERTAUT, E. F. (1972). *Z. Kristallogr.* **136**, 98–105.
BLESS, P. W. & KOSTINER, E. (1973). *J. Solid State Chem.* **6**, 80–85.
CALABRESE, J. C. & BURNETT, R. M. (1980). *TAPER.* Locally modified version by Z. TUN, with the permission of the Nicolet XRD Corporation.
CALVO, C. & FAGGIANI, R. (1975). *Can. J. Chem.* **53**, 1516–1520.
DACHILLE, F. & ROY, R. (1960). *Am. J. Sci.* **258**, 225–246.
DAVIS, R. J., HEY, M. H. & KINGSBURY, A. W. G. (1965). *Mineral. Mag.* **35**, 72–83.
ENGEL, G. & KLEE, W. E. (1970). *Z. Kristallogr.* **132**, 332–339.
FLEET, M. E. & BARBIER, J. (1988). *Acta Cryst.* C**44**, 232–234.
FLEET, M. E. & BARBIER, J. (1989). *Acta Cryst.* B**45**, 201–205.

FRENCH, S. & WILSON, K. (1978). *Acta Cryst.* A**34**, 517–525.
GOPAL, R., RUTHERFORD, J. S. & ROBERTSON, B. E. (1980). *J. Solid State Chem.* **32**, 29–40.
HALL, S. R. & STEWART, J. M. (1989). Editors. *XTAL2.6 User's Manual.* Univs. of Western Australia, Australia, and Maryland, USA.
HAWTHORNE, F. C. (1986). *Am. Mineral.* **71**, 206–209.
HENSEN, B. J. (1977). *Phys. Earth Planet. Inter.* **14**, P3–P5.
HYDE, B. G., WHITE, T. J., O'KEEFFE, M. & JOHNSON, A. W. S. (1982). *Z. Kristallogr.* **160**, 53–62.
JOUBERT, J. C. & DURIF, A. (1964). *Bull. Soc. Fr. Mineral. Cristallogr.* **87**, 47–49.
KRISHNAMACHARI, N. (1970). PhD Thesis, Department of Chemistry, McMaster Univ., Canada.
KRISHNAMACHARI, N. & CALVO, C. (1970*a*). *Can. J. Chem.* **48**, 3124–3131.
KRISHNAMACHARI, N. & CALVO, C. (1970*b*). *Can. J. Chem.* **48**, 881–889.
KRISHNAMACHARI, N. & CALVO, C. (1971). *Can. J. Chem.* **49**, 1629–1637.
KRISHNAMACHARI, N. & CALVO, C. (1973). *Acta Cryst.* B**29**, 2611–2613.
KRISHNAMACHARI, N. & CALVO, C. (1974). *Can. J. Chem.* **52**, 46–50.
MOORE, P. B. (1972). *Am. Mineral.* **57**, 24–35.
OZOG, J., KRISHNAMACHARI, N. & CALVO, C. (1970). *Can. J. Chem.* **48**, 388–389.
PALAZZI, M. & GUÉRIN, H. (1978). *Bull. Soc. Chim. Fr.* pp. I119–I120.
POULSEN, S. J. & CALVO, C. (1968). *Can. J. Chem.* **46**, 917–927.
SAUERBREI, E. E., FAGGIANI, R. & CALVO, C. (1973). *Acta Cryst.* B**29**, 2304–2306.
SHANNON, R. D. & CALVO, C. (1972). *Can. J. Chem.* **50**, 3944–3949.
TAYLOR, J. B. & HEYDING, R. D. (1958). *Can. J. Chem.* **36**, 597–606.

Acta Cryst. (1991). B**47**, 462–468

Structural and Thermal Parameters for Rutile and Anatase

BY C. J. HOWARD

Australian Nuclear Science and Technology Organisation, Lucas Heights Research Laboratories, Private Mail Bag 1, *Menai, New South Wales* 2234, *Australia*

AND T. M. SABINE AND FIONA DICKSON*

University of Technology, Sydney, PO Box 124, *Broadway, New South Wales* 2007, *Australia*

(*Received* 6 *September* 1990; *accepted* 12 *March* 1991)

Abstract

Neutron powder diffraction patterns from rutile (TiO_2, $P4_2/mnm$, $a = 4{\cdot}594$, $c = 2{\cdot}959$ Å) and anatase (TiO_2, $I4_1/amd$, $a = 3{\cdot}785$, $c = 9{\cdot}514$ Å) have been analysed by the Rietveld method. The positional parameters were determined to be $x_O = y_O = 0{\cdot}30478$ (6) in rutile and $z_O = 0{\cdot}20806$ (5) in anatase. The anisotropic thermal parameters were also determined. The results from this constant-wavelength neutron diffraction study are in remarkably good agreement with the results from a recently published analysis of time-of-flight neutron data from the same phases. A comparison is made with results from earlier X-ray single-crystal investigations of these polymorphs of titania, and again the agreement is good. In particular, there is no evidence for any significant difference between X-ray and neutron determinations of the oxygen position such as might have resulted from polarization effects. The thermal vibrations show marked anisotropy, which appears to be determined by the stereochemistry of the crystal structure. The Debye temperatures estimated from the diffraction data are 600 (10) K for rutile and 520 (10) K for anatase at room temperature.

1. Introduction

The crystal structures of rutile and anatase, two of the polymorphs of titanium dioxide, were first described by Vegard (1916). The structures have been redetermined from time to time, using improved techniques to obtain more accurate crystal structure data. These additional investigations have been motivated by interests in the electronic properties, the nature of the bonding, and the general relationship between electronic properties and crystal structure in these materials. The further work includes an X-ray powder diffraction study of anatase and rutile (Cromer & Herrington, 1955), single-crystal X-ray diffraction investigations of anatase (Horn, Schwerdtfeger & Meagher, 1972) and of rutile (Abrahams & Bernstein, 1971; Shintani, Sato & Saito, 1975; Gonschorek, 1982), and neutron diffraction investigations of rutile using both single-crystal (Gonschorek & Feld, 1982) and powder (Sabine & Howard, 1982) techniques. For rutile,

* Present address: Bristows Cooke and Carpmael, 10 Lincoln's Inn Fields, London WC2A 3BP, England.

0108-7681/91/040462-07$03.00